The Transferrin Receptor: A Potential Molecular Imaging Marker for Human Cancer[1]

Dagmar Högemann-Savellano, Erik Bos†, Cyrille Blondet*,‡, Fuminori Sato*,‡, Tatsuya Abe*,‡, Lee Josephson*, Ralph Weissleder*, Justin Gaudet§, Dennis Sgroi§, Peter J. Peters† and James P. Basilion*,‡*

*Center for Molecular Imaging Research, Massachusetts General Hospital, Charlestown, MA, USA; †Netherlands Cancer Institute, Antoni van Leeuwenhoek Hospital, Plesmanlaan 121-H4, Amsterdam 1066 CX, The Netherlands; ‡NFCR-Center for Molecular Analysis and Imaging and §Molecular Pathology Unit, Massachusetts General Hospital, Charlestown, MA, USA

Abstract

Noninvasive imaging of differences between the molecular properties of cancer and normal tissue has the potential to enhance the detection of tumors. Because overexpression of endogenous transferrin receptor (TfR) has been qualitatively described for various cancers and is presumably due to malignant transformation of cells, TfR may represent a suitable target for application of molecular imaging technologies to increase detection of smaller tumors. In the work reported here, investigation into the biology of this receptor using electron microscopy has demonstrated that iron oxide particles targeted to TfR are internalized and accumulate in lysosomal vesicles within cells. Biochemical analysis of the interaction of imaging probes with cells overexpressing the TfR demonstrated that the extent of accumulation, and therefore probe efficacy, is dependent on the nature of the chemical cross-link between transferrin and the iron oxide particle. These data were utilized to design and synthesize an improved imaging probe. Experiments demonstrate that the novel magnetic resonance imaging (MRI) probe is sensitive enough to detect small differences in endogenous TfR expression in human cancer cell lines. Quantitative measurement of TfR overexpression in a panel of 27 human breast cancer patients demonstrated that 74% of patient cancer tissues overexpressed the TfR and that the sensitivity of the new imaging agent was suitable to detect TfR overexpression in greater than 40% of these cases. Based on a biochemical and cell biological approach, these studies have resulted in the synthesis and development of an improved MRI probe with the best *in vitro* and *in vivo* imaging properties reported to date.

Neoplasia (2003) **5**, 495–506

Keywords: Transferrin receptor, molecular imaging, CLIO, breast cancer, electron microscopy.

Introduction

A major goal for the field of molecular imaging has been real-time noninvasive detection of gene expression *in vivo*. A significant amount of effort in this field has been directed at imaging transgenes, with cDNA being added to the complement of normally expressed genes in target tissues (for review, see Ref. [1]). Following gene transfer, specific probes designed to exploit the unique characteristics of transferred gene products are used to report on transgene expression. Examples of such imaging successes include luciferase (optical imaging [2,3]), the thymidine kinase of herpes simplex virus I (HSV-TK; nuclear imaging [4]), and β-galactosidase (magnetic resonance imaging, MRI [5]). Many of the achievements of these strategies have been due to the use of transgenes that have little or no expression in the targeted tissues, or even the species under investigation. Therefore, translations of these imaging successes into common utility require pairing of the technologies with transgenic animals or gene therapy.

On the other hand, significant accomplishments have also been demonstrated for imaging endogenous gene products, whose expression and/or activity is altered in the disease state (for review, see Ref. [6]). In our own work using MRI to noninvasively image transgene expression *in vivo*, we have attempted to merge transgene and endogenous gene imaging approaches. Utilizing the engineered transferrin receptor (ETR) derived from an endogenous gene, the transferrin receptor (TfR), we have relied on the resolution of MRI and ETR-targeted iron oxide probes to image the expression of the transferred ETR [7–9]. This version of the receptor is identical at the protein level but lacks *cis*-acting RNA elements, thus allowing constitutively high levels of TfR protein expression. This approach has demonstrated the utility of MRI to image transgene expression and has also shown that it is feasible to image relative differences in receptor expression [7,9,10]. These findings have suggested a number of possibilities for application of MRI to monitor disease-specific changes in endogenous TfR expression. For example, overexpression of

Address all correspondence to: James P. Basilion, PhD, Center for Molecular Imaging Research, Massachusetts General Hospital, Building 149 13th Street, No. 5406, Charlestown, MA 02129, USA. E-mail: basilion@helix.mgh.harvard.edu

[1]This work was, in part, funded by a grant from the National Cancer Institute (grant no. RO1 CA85240), the Department of Defense Concept Award, an Avon Grant, and the National Foundation for Cancer Research. D.H.S. received a fellowship from the Deutsche Forschungsgemeinschaft, Germany

Received 14 May 2003; Revised 3 October 2003; Accepted 8 October 2003.

endogenous TfR has been qualitatively described for various cancers [11–15], presumably due to malignant transformation of normal cells, and therefore TfR may represent a suitable target for early detection of cancer.

Our previous work [7–9] demonstrating the feasibility of imaging the TfR also highlighted the need for synthesis of probes with improved sensitivity to image changes in endogenous TfR expression. The goal of this study was to utilize the biochemical analysis of transferrin (Tf)–iron oxide–cell interactions to improve the synthesis and design of a more sensitive MR probe for the TfR. In order to design a more efficacious MRI probe, we have 1) investigated in detail the biology of TfR-targeted iron oxide imaging probes; 2) applied this knowledge to synthesize more efficacious probes; 3) demonstrated the utility of the new probes; and 4) validated the utility of the TfR to be an informative imaging marker for human breast cancer. Specifically, the current work demonstrates that: 1) iron oxide particles are internalized and sorted to lysosomal vesicles within cells; 2) the chemical cross-link used for the covalent binding of Tf and iron oxide particles has an influence on the biology of particle internalization; 3) the nature of cross-linking can improve the efficacy of the probe for TfR/ETR imaging *in vitro* and *in vivo*; and 4) the improved probe can be utilized to image small differences in endogenous TfR expression in human cancer cell lines. Finally, to show the utility of endogenous TfR as a marker for human cancers, the level of endogenous TfR overexpression was quantified in over 25 human breast cancer patients, demonstrating that a large proportion of these patients significantly overexpresses endogenous TfR in their cancer tissues.

Experimental

Synthesis of TfR-Targeted Iron Oxide Particles

Monocrystalline iron oxide nanoparticles were prepared through the reaction of iron salts with ammonium hydroxide in the presence of T10 dextrans [16]. The dextrans were then modified in the presence of epichlorohydrin according to previous reports to yield cross-linked iron oxide nanoparticles (CLIO-10). CLIO was finally treated with ammonia and dialyzed as described, in order to obtain reactive groups for the covalent binding of bifunctional linker reagents [17].

The conjugation of CLIO-NH_2 and human diferric Tf (Sigma, St. Louis, MO) using the linker reagent *N*-succinimidyl 3-(2-pyridyldithio)propionate (SPDP; Molecular Biosciences, Boulder, CO) leads to a disulfide bond (Tf-SS-CLIO) [8], whereas employing the linker reagent succinimidyl iodoacetate (SIA; Molecular Biosciences) forms a more stable covalent linkage through a thioether bond (Tf-SC-CLIO) [18]. The synthesis of Tf-SS-CLIO and Tf-SC-CLIO is summarized in Figure 1 and has been described before [8,18]. Unreacted Tf-SH was separated from Tf-SS-CLIO and Tf-SC-CLIO using magnetic columns (Macs separation columns; Miltenyi Biotech, Auburn, CA) equilibrated with phosphate-buffered saline (PBS; pH 8). To calculate the number of Tf molecules per particle, the protein (BCA; Pierce, Rockford, IL) and iron concentrations of purified material were determined [10,19] and a mean of 2064 iron atoms per particle was assumed [19]. The r_1 and r_2 relaxivities were measured using a 0.47 T tabletop minispectrometer, as described [19]. The conjugates were stored in PBS, pH 8, either at 4°C, or were shock-frozen in liquid nitrogen and kept at −20°C.

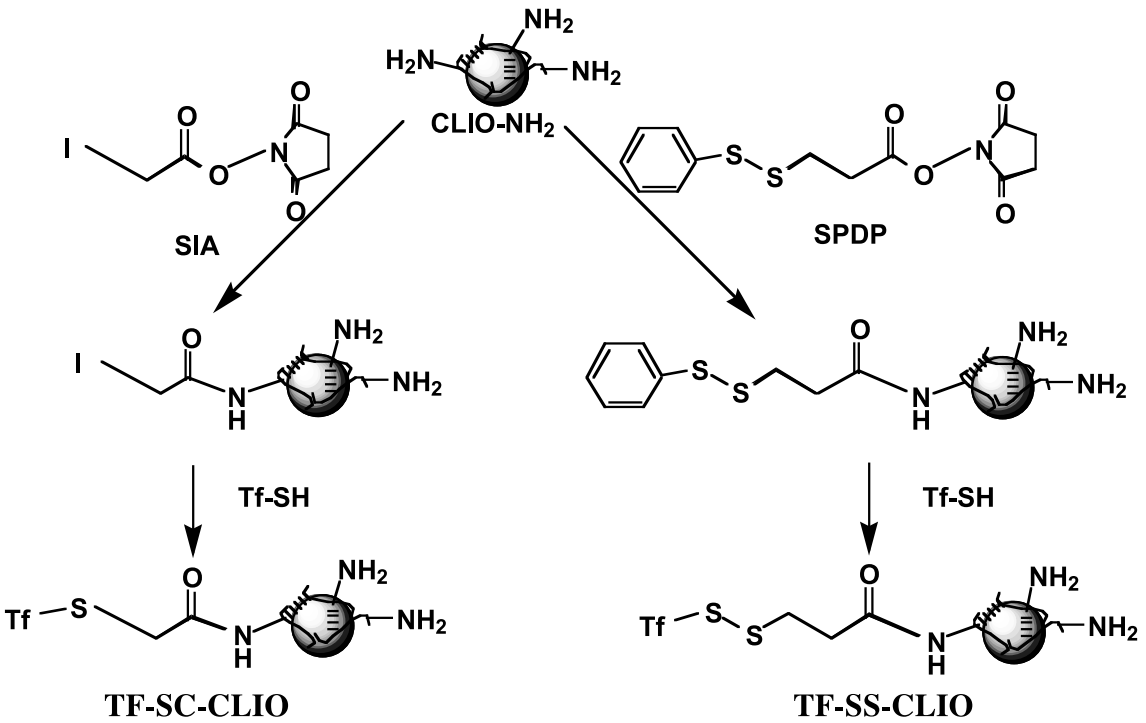

Figure 1. *Reaction schemes for the synthesis of Tf-SS-CLIO and Tf-SC-CLIO.*

Cell Culture

Wild-type rat 9L gliosarcoma cells (Brain Tumor Research Center, San Francisco, CA) and rat 9L gliosarcoma cells stably transfected with an altered form of the human transferrin receptor ETR (9L3.9 and 9L4.2 cells) [7,10] were grown in Dulbecco's modified Eagle's medium (DMEM) (Cellgro; Mediatech, Washington, DC) containing 10% fetal bovine serum (FBS; Cellgro). Transfected cells were periodically passaged in the presence of G418 to assure the integrity of plasmid expression [10]. Breast carcinoma cell lines BT20, MCF7, BT549, and HBL100 as well as the nontumorigenic cell line MCF10A derived from fibrocystic disease were obtained from the ATCC (Manassas, VA) and kept in culture as recommended. In all cell cultures, the medium was changed every third day and cells were split at a confluence of about 80%.

Analysis of TfR Expression by Western Blotting

Samples of 10^6 cells were heated for 5 minutes in 80 μl of sodium dodecyl sulfate (SDS) sample buffer containing 5% β-mercaptoethanol and then passaged through a 28-gauge needle. Equal amounts (20 μl/lane) were separated on 8% SDS polyacrylamide gels [20] and transferred onto Hybond-P membranes (Amersham Biosciences, Piscataway, NJ). Immunoblot analyses were performed using an ECL kit (Amersham Biosciences) according to the manufacturer's instructions. In brief, after blocking with 5% dry milk in TBS-T [20 mM Tris–HCl (pH 7.5), 150 mM NaCl, 0.1% Tween 20], the membranes were incubated for 2 hours at room temperature with the primary anti–TfR antibody (H68.4; Zymed Laboratories, Inc., San Francisco, CA) diluted 1:500 in TBS-T containing 5% dry milk. After washing in TBS-T, the membranes were incubated for 1 hour at room temperature with horseradish peroxidase–conjugated anti–mouse secondary antibodies (Sigma) at a concentration of 1:10000 in TBS-T containing 5% dry milk. The membranes were then washed thoroughly in TBS-T, swirled for 1 minute in ECL reagents, and exposed to photographic films. For assessment, films were scanned and the number of pixels in regions of interest was quantified using NIH Image 1.6. Because no preflashing of the films was carried out, the data can only be described as semiquantitative. Reported data have been corrected for background intensities.

Competition and Uptake Studies with Radioactively Labeled Tf

Tf was radiolabeled with $Na^{125}I$ in the presence of IodoGen (Pierce). Unbound iodide was removed by centrifugation through Bio-Gel P6 spin columns (Bio-Rad, Hercules, CA). Cells were plated at a density of 10^5 cells/well onto 24-well plates (Falcon; Becton Dickinson, Lincoln Park, NJ). One day (9L3.9) or 2 days (BT20, MCF7, BT549, HBL100, and MCF10A) later, different concentrations of unlabelled diferric Tf, Tf-SS-CLIO, or Tf-SC-CLIO (2.5 nM–2.5 μM Tf in DMEM) were added immediately prior to the addition of [^{125}I]Tf (0.25 nM in DMEM) and cells were incubated for 1 hour at 37°C. The cells were then washed three times with Hanks' balanced salt solution (HBSS; Bio-Whittaker, Walkersville, MD) and detached with trypsin (0.05% trypsin, 0.5 mM ethylenediaminetetra-acetic acid). The entire contents of the wells were counted in a γ-counter (1282 Compugamma CS; LKB Wallac, Turko, Finland) to determine cell-associated radioactivity.

Stability of TfR-Targeted Iron Oxide Particles in Cell Culture

9L3.9 cells were plated in 24-well dishes at a density of 10^5 cells/well. Twenty-four hours later, cells were washed with HBSS and incubated with Tf-SS-CLIO or Tf-SC-CLIO (0.375 μM/ml Tf) in DMEM alone or DMEM containing the metabolic inhibitors 50 mM 2-deoxy-D-glucose, 1% Na-azide, and 10 mM KCN [21]. Both conjugates were also incubated in cell-conditioned DMEM (conditioned for 6 hours), or in fresh DMEM. All incubations were carried out for 6 hours at 37°C. SDS polyacrylamide gel electrophoresis [20] was used to determine the integrity of the different conjugates. Samples were mixed with nonreducing SDS sample buffer. Where reducing conditions were used, 5% β-mercaptoethanol was added to the SDS sample buffer and samples were heated at 95°C for 5 minutes. Nonreduced samples were not subjected to heating as controls demonstrated that this had no effect on the integrity of the conjugate (data not shown). Three micrograms of protein was loaded per lane and separated using a 10% SDS polyacrylamide gel. Gels were run at a constant voltage of 120 V and stained with Coomassie brilliant blue R-250.

Electron Microscopy (EM)

One day prior to treatments, 9L3.9 cells were seeded at a density of 10^6 cells per 10-cm culture dish. Cells were then incubated in the indicated medium for 2, 24, and 48 hours, respectively, and were washed three times with cell-conditioned medium. Afterward, cells were fixed by adding to the culture medium an equal volume of 0.2 M PHEM buffer (120 mM PIPES, 50 mM HEPES, 4 mM $MgCl_2$, 20 mM EGTA; pH 6.9) containing 0.4% paraformaldehyde and 2% glutaraldehyde. After fixation for 1 hour at room temperature, cells were rinsed in PBS, scraped with a rubber policeman into 5 ml of PBS containing 1% gelatin, and pelleted at 700 rpm for 10 minutes (Sorvall 7 RT; Kendro Laboratory Products, Newtown, CT). The cells were resuspended in 2 ml of PBS, pelleted again at 700 rpm for 10 minutes, and taken up into storage buffer (0.5% paraformaldehyde in 0.1 M PHEM buffer). For immunogold labeling, the buffer was replaced by PBS containing 20 mM glycine. Cells were then embedded in 12% gelatin in phosphate buffer, infiltrated for 4 hours in 2.3 M sucrose in the same buffer, and frozen in liquid nitrogen. Ultrathin sectioning (60 nm) and immunogold labeling were carried out as described elsewhere [22]. Anti–human TfR antibody (H68.4) was purchased from Zymed Laboratories, Inc. The immunogold-labeled sections were incubated for 5 minutes on a drop of distilled water containing 2% methylcellulose and 0.4% uranyl acetate, after which they were air-dried. In some experiments, cell contrast was reduced in order to distinguish the electron-dense CLIO particles from the surrounding cytoplasm. In those cases, the immunogold-labeled sections were incubated for 5 minutes on a drop of

distilled water containing 2% methylcellulose and 0.4% uranyl acetate. Then, the sections were rinsed for 10 minutes on a drop of distilled water, put on a drop of 2% methylcellulose for 5 minutes, and air-dried. The sections were examined in the transmission electron microscope at 80 kV and photographed at a magnification of × 21,000.

MRI In Vitro

Concentration-dependent cell association, time course, and washout studies To determine the cellular association of Tf-targeted CLIO conjugates, 10^5 cells were seeded per well onto 24-well plates 1 day (9L3.9) or 2 days (BT20, MCF7, BT549, HBL100, and MCF10A) before the experiment. Cells were then incubated for 2 hours in DMEM, 10% FBS containing either Tf-SS-CLIO or Tf-SC-CLIO at increasing concentrations (1.8 μM–3.6 mM iron). For time-dependent studies, 3.5×10^4 cells (9L3.9) were seeded onto 24-well plates. Twenty-four hours later, the cells were incubated for 2, 8, 24, or 48 hours with either Tf-SS-CLIO or Tf-SC-CLIO (3.6 mM iron) in DMEM, 10% FBS. For washout experiments, cells (9L3.9) were loaded for 18 hours with Tf-SS-CLIO or Tf-SC-CLIO (3.6 mM iron) in DMEM, 10% FBS, washed once with HBSS, and the medium was changed to fresh DMEM, 10% FBS. Cells were harvested at time zero (immediately after washing) and 2, 8, and 24 hours after cessation of loading. To control for receptor specificity, cells were also incubated with nonconjugated CLIO (3.6 mM iron) as well as with Tf-SS-CLIO or Tf-SC-CLIO (3.6 mM iron) in the presence of a 10-fold excess of nonconjugated Tf. Nonspecific binding of the probes to culture dishes was measured by the incubation of probe in the absence of cells.

Cell harvesting All incubations were carried out at 37°C and at the end of the respective incubation times and conditions, cells were washed three times with HBSS and then lysed in 60 μl of PBS, pH 8, containing 1% Triton X-100. Lysates were transferred to the wells of 384-well plates and centrifuged at 700 rpm for 2 minutes (Sorvall 7 RT; Kendro Laboratory Products) to remove any air bubbles trapped at the bottom of the wells. Purified CLIO particles (0.9–18 μM iron/ml PBS, pH 8, 1% Triton X-100) were also included in the dish as standards.

MR measurements MRI was performed using a clinical 1.5 T superconducting magnet (Signa 5.0; GE Medical Systems, Milwaukee, WI) equipped with a standard 3- or 5-in. surface coil. MRI and postprocessing of the data have been described before [18]. In brief, the imaging protocol consisted of a spin echo sequence (TR 3000 milliseconds, variable TE 15–1200 milliseconds; total of 20–24 echo times). At a field of view (FOV) of 8 cm × 8 cm, a 256 × 256 imaging matrix, and a slice thickness of 1.5 mm, each voxel had a size of 0.146 mm^3. The obtained MR images were processed on a personal computer using MATLAB 6.0 (The MathWorks, Natick, MA). Signal intensities of each single voxel were plotted against the various echo times (TEs) and curve fitting for exponential decay allowed the calculation of T_2 relaxation times according to the following equation: $SI = Ae^{(-T\varepsilon/T_2)} + B$, with SI = signal intensity, TE = echo time, A = amplitude, and B = offset. For the automatic measurement of the average T_2 relaxation time of each well, the software IPLab 3.5.2 (Scanalytics, Fairfax, VA) was used and the data were exported to a spreadsheet [18].

MRI In Vivo

Clones of 9L gliosarcoma cell lines differing in their expression of the TfR (9L3.9 and 9L4.2) were cultivated in 175-cm^2 culture flasks [7]. Cells were detached, washed with HBSS, and resuspended in HBSS at a concentration of 6×10^4 cells/μl. Nude mice (nu/nu; Fisher Scientific, Agawam, MA) were anesthesized by intraperitoneal injection of ketamine (80 mg/kg; Parke-Davis, Morris Plains, NJ) and xylazine (12 mg/kg; Miles, Shawnee Mission, KS) and tumor cells were implanted subcutaneously at the base of the ear ($n = 8$).

Based on preliminary studies, implantation at the base of the ears was chosen as the best model because: 1) tumors were highly vascularized; 2) symmetric placement was easily achieved; and 3) tumors grew at a similar rate, reaching a comparable size sufficient for MRI. MR examinations were performed using a 1.5-T MR imager (Signa 5.0; GE Medical Systems) employing a special 1.5-in. surface coil (Nova Medical, Inc., Wakefield, MA). All sequences had the same resolution with a FOV of 5 cm × 2.5 cm (Phase FOV 0.5), a 256 × 160 imaging matrix, and a slice thickness of 1.5 mm. Localizers in all three planes allowed the exact placement of the imaging slices. The intravenous dose of contrast agent, 15 mg iron/kg body weight, was determined empirically. The spin echo sequences used were: 1) TR 300 milliseconds, TE 11 milliseconds, four NEX, 1:40 minutes; and 2) TR 2000 milliseconds, TE 15, 25, 30, 45, 50, 60, 75, and 100 milliseconds, one NEX, 6:08 minutes. For Fast Spin Echo Inversion Recovery, the following parameters were used: TR 4850 milliseconds, effective TE 36 milliseconds, TI 150 milliseconds, two NEX, 1:42 minutes.

Five days after implantation, MR images were obtained and contrast probes were administered by tail vein injection (Tf-SC-CLIO, $n = 4$, or nonconjugated CLIO, $n = 4$). MRI was repeated 24, 48, and 72 hours after contrast agent. T_2 maps were calculated using MATLAB 6.0, as previously described. After the MRI examinations, animals were kept alive for another week to harvest enough tumor tissues for the analysis of TfR expression by Western blotting. Under general anesthesia, mice were sacrificed by lethal intravenous injection of sodium pentobarbital (200 mg/kg; Anpro, Arcadia, CA). Each tumor was directly transferred into 3 ml of ice-cold MES buffer (0.1 M MES, 1 mM EGTA, 0.5 mM $MgCl_2$; pH 6.5) and homogenized using a glass Teflon homogenizer. After centrifugation for 20 minutes at 12,000 rpm (Sorvall, SS 34 Rotor; Kendro Laboratory Products), the supernatants were collected and centrifuged for 1 hour at 26,000 rpm (Ti 45 Rotor; Beckman, Columbia, MD). Each resulting pellet was resuspended in 150 μl of MES buffer. The protein content was determined using a BCA Assay (Pierce), all samples were diluted to a protein concentration of 2.7 μg/ml, and mixed 1:2 with reducing SDS sample buffer. Forty microliters per lane

were separated by SDS gel electrophoresis and the TfR expression was analyzed by Western blotting (see above).

Laser Capture Microdissection and Real-Time Quantitative Polymerase Chain Reaction (RT-Q-PCR)

For procured samples, we have used laser capture microdissection with a PixCell II LCM Microscope (Arcturus Engineering, Mountain View, CA) to collect normal and cancer cells from fresh frozen tumor sections derived from patient samples. RNA was then isolated from dissected cells, linearly amplified, and expression of the TfR mRNA was quantified by RT-Q-PCR. Procedures are detailed in Sgroi et al. [23]. All human samples were obtained and experiments were conducted with IRB-approved protocols.

Results

Type of Conjugation Affects Cellular Uptake of Contrast Agents

Previously, we described a model in which overexpression of the engineered version of the TfR (ETR) in cells results in binding and presumably internalization of a derivatized form of holotransferrin. In those studies, it was demonstrated that the proposed model is valid for noninvasive imaging of ETR transgene expression by MRI using Tf conjugated with iron oxide nanoparticles [7,8,10]. In order to better understand the underlying biological mechanisms resulting in improved detection by MRI and to apply this knowledge to image changes in endogenous TfR expression, the molecular events that occur upon interaction of derivatized Tf with cells were investigated. For these studies, two different conjugation schemes were used. The first formed disulfide linkages between Tf and iron oxide particles [8] and the second formed thioether bonds [18]. Both conjugation procedures are summarized in Figure 1.

First it was determined if different conjugation strategies affected the affinity of the Tf–iron oxide molecules for the receptor. Previous studies showed a significant increase in affinity with altered linker chemistry and length [8]. However, here, little difference was found in the affinity of Tf-SS-CLIO and Tf-SC-CLIO for TfR. Normalized to total particles present, the IC_{50} was 84 ± 5.9 nM for Tf-SS-CLIO and 126.5 ± 19.5 nM for Tf-SC-CLIO. Normalized to Tf molecules, the IC_{50} of Tf-SS-CLIO is 306.8 ± 21.2 nM (see Ref. [8]) and the IC_{50} of Tf-SC-CLIO is 184.1 ± 28.4 nM. The magnetic properties of Tf-SS-CLIO and Tf-SC-CLIO were also very similar and are summarized in Table 1.

Table 1. Properties of Tf–Iron Oxide Conjugates.

Compound	r_1 [sec × mM]$^{-1}$	r_2 [sec × mM]$^{-1}$	Average Tf Molecules Per Particle	Linker Chemistry
Tf-SS-CLIO (n = 4)	31.2 ± 0.5	149.1 ± 8.8	3–4	Disulfide bond
Tf-SC-CLIO (n = 4)	32.1 ± 2.7	144.0 ± 6.1	1–2	Thioether bond

However, as expected, the chemical stability of the linkers differed. SDS gel electrophoresis revealed that the Tf-SC-CLIO conjugate, unlike the Tf-SS-CLIO conjugate, remained intact following treatment with 5% β-mercaptoethanol (Ref. [8] and data not shown). The different chemical stability of the linkers affected the interaction of the conjugates with cells. In comparison to the controls, increased amounts of free Tf were detected after incubation of Tf-SS-CLIO with either tissue culture cells or cell-conditioned DMEM, the latter suggesting that disulfide bond cleavage could occur in the absence of cells (Figure 2, *right panel*). In contrast, no Tf was liberated when incubations were performed with Tf-SC-CLIO (Figure 2, *left panel*). For Tf-SS-CLIO, cleavage of the disulfide bond was also observed after incubation with cells in the presence of metabolic inhibitors of cellular uptake (10 mM KCN, 1% Na-azide, and 50 mM 2-deoxy-D-glucose; see Experimental section), further indicating that cellular internalization is not required for cleavage of Tf-SS-CLIO (data not shown).

When the cellular uptake of the conjugates was investigated, it was determined that the type of linkage significantly affected the uptake, but not the efflux, of the Tf-targeted iron oxide particles. Even though the two conjugates had similar affinities for the TfR, the concentration dependence and time course for uptake varied significantly. At both lower concentrations (Figure 3*A*) and at shorter times (Figure 3*B*), the extent of cell-associated iron oxide particles (as measured by MRI) was greater with the more stable probe, Tf-SC-CLIO. The most significant binding and uptake of both conjugates were seen in the first 2 hours with a continuingly higher cellular accumulation of iron for Tf-SC-CLIO over an extended time course (Figure 3*B*). The improved uptake of Tf-SC-CLIO by cells was not due to an effect of linker chemistry on the efflux of iron oxide nanoparticles from the cells (Figure 4). Between 2 and 8 hours after incubation with Tf-targeted CLIO, the washout of iron oxides was complete and reached a plateau for both conjugates of 41.1 ± 3.7% of starting values.

Analysis of Uptake by EM

The difference in uptake of iron oxide particles depending on the linker chemistry of the conjugates was also reflected by EM. Using nanogold-conjugated antibodies specific to structural markers or the TfR, EM was used to determine the subcellular location of TfR and CLIO particles. Panel A in Figure 5 presents the pattern of TfR distribution in 9L3.9 cells that were not incubated with either of the imaging probes. Gold particles indicating the location of the TfR are seen in association with the plasma membrane, coated vesicles, endosomes, and the Golgi complex. Panels B and C show that after 2 hours of incubation with Tf-SC-CLIO conjugates, CLIO particles were often localized within large TfR-positive structures, characteristic for late endosomes (CLIO particles, due to their density and size, are readily visible without gold-conjugated antibodies). After 48 hours of incubation with Tf-SC-CLIO conjugates, CLIO particles accumulated in lysosomes (l), as demonstrated in panels D, E, and F (arrowheads). In contrast to panels B and C, only small amounts of gold particles (indicating the presence of TfR) and CLIO

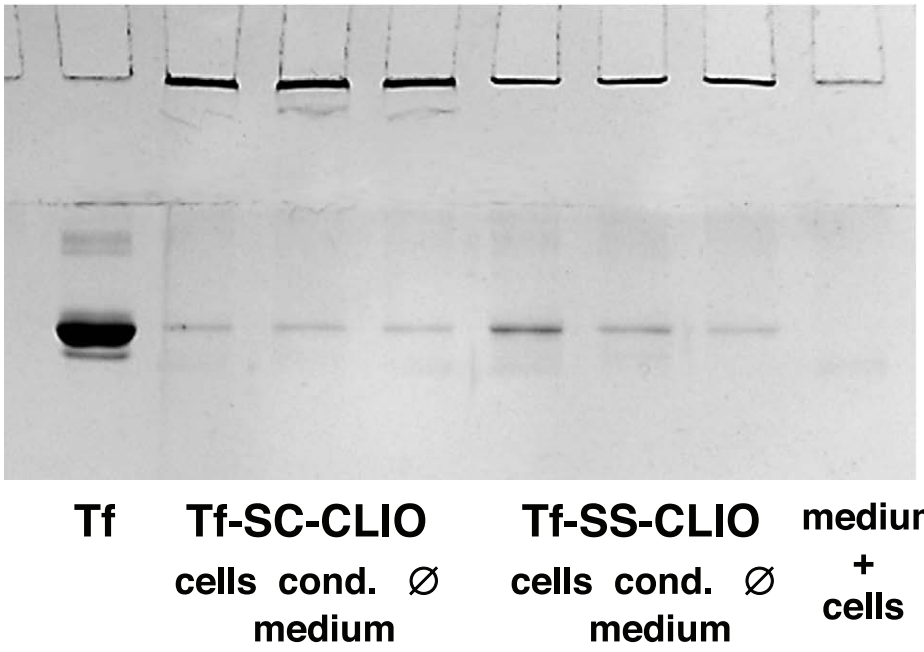

Figure 2. *Stability of MRI probes. SDS gel electrophoresis was used to determine the stability of the conjugates to different treatments. Conjugates were incubated in tissue culture dishes containing DMEM and cells, cell-conditioned DMEM, or DMEM alone. Following incubation, a portion of the medium was subjected to electrophoresis. Lane 1 is holotransferrin for reference and lane 8 is medium from a well that contained cells and DMEM, but was not incubated with probe.*

particles were contained in endosomes in panels D, E, and F (a large translucent endosome can be seen in photo F). From these data, it would appear that most Tf-SC-CLIO uptake occurs within the first 2 hours and slows down over time (Figure 3*B*). In comparison to the 2-hour time point, the amount of TfR and CLIO particles in endosomes seen by EM decreased after a continuous 48-hour incubation with Tf-SC-CLIO. Because no signs of iron toxicity were noted, it is

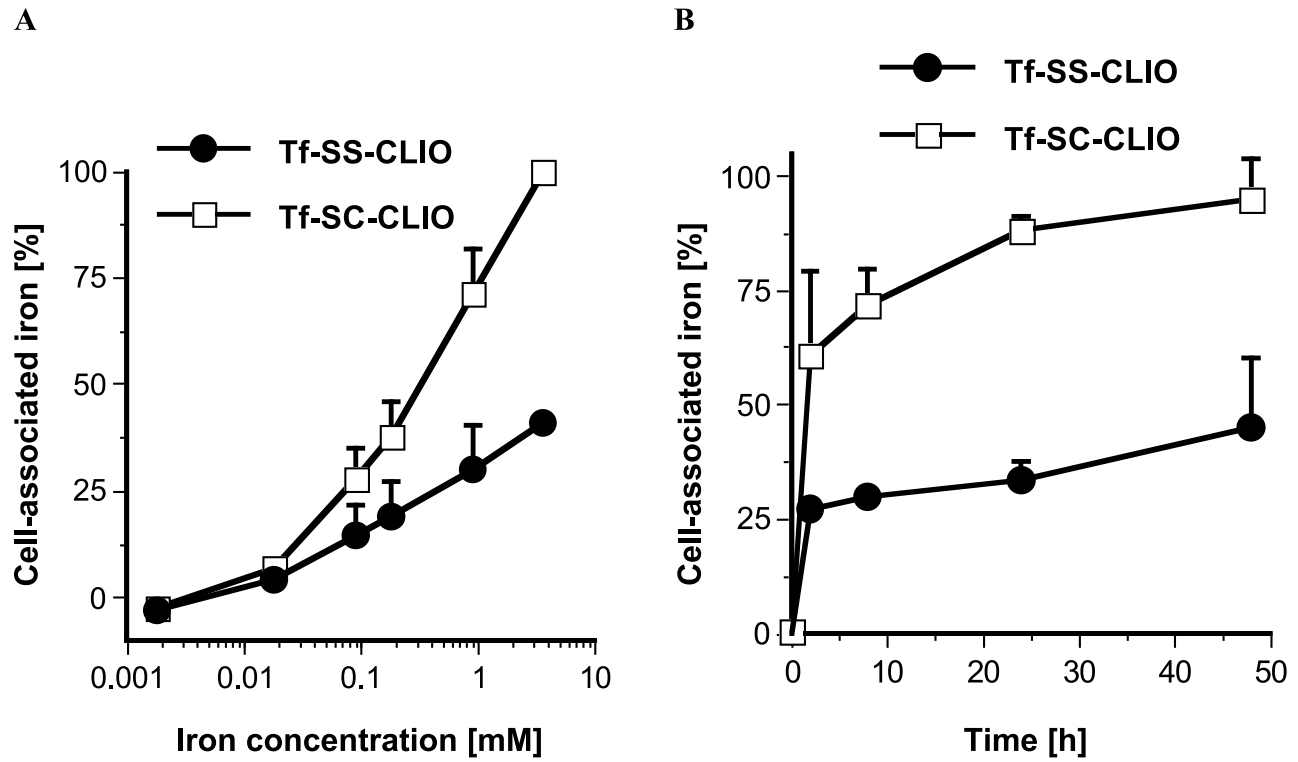

Figure 3. *Cell-associated iron after incubation with Tf-SS-CLIO or Tf-SC-CLIO. Cells (9L3.9) were incubated with increasing concentrations of the two conjugates for 2 hours (A) or with saturating concentrations (3.6 mM iron) for the indicated times (B). Following incubations, cells were washed with HBSS, lysed, and imaged by MRI. Iron contents were calculated based on standards of purified CLIO and expressed in relation to the highest iron concentration found in each experiment (maximum concentration or maximum time). Data are presented as the mean and standard deviation of quadruplicates.*

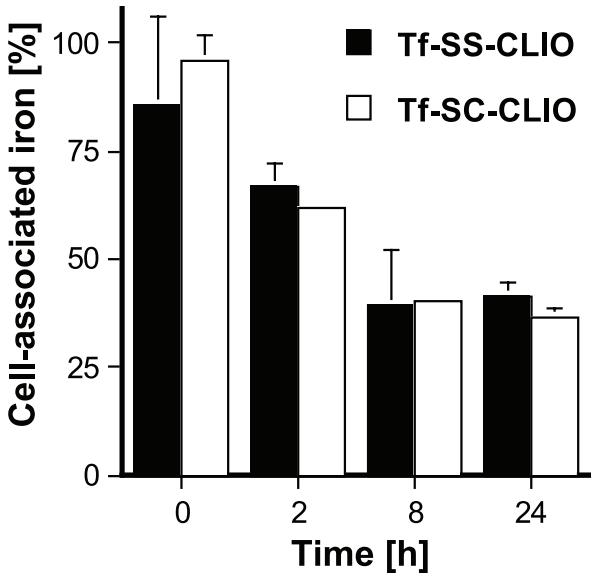

Figure 4. *Washout of cell-associated iron oxide particles after incubation with Tf-SS-CLIO or Tf-SC-CLIO. Cells (9L3.9) were incubated with saturating concentrations (3.6 mM iron) of either conjugate for 18 hours, then washed with HBSS, and incubated with fresh medium. At the indicated times, cells were again washed with HBSS, lysed, and imaged by MRI. Iron contents were calculated based on standards of purified CLIO and expressed as a percentage of the highest iron concentration found after incubation with Tf-SS-CLIO or Tf-SC-CLIO, respectively. Data are presented as the mean and standard deviation of quadruplicates.*

likely that the potential explanation for this finding is that TfR recycling is interrupted, which eventually leads to a depletion of TfR and therefore a decreased uptake of Tf-targeted CLIO. Cells challenged with Tf-SS-CLIO showed overall a very similar pattern of TfR and CLIO distribution, but a considerably smaller number of internalized CLIO particles than cells challenged with Tf-SC-CLIO (data not shown). The relative amounts of internalized CLIO particles were estimated by EM after incubation with probes and are as follows: Tf-SC-CLIO (2 hours), Tf-SC-CLIO (48 hours), Tf-SS-CLIO (2 hours), Tf-SS-CLIO (48 hours), 20:30:5:10, respectively.

Imaging Differences in TfR Expression In Vitro and In Vivo

The Tf-SC-CLIO probe was shown to have a better ability to image TfR expression by MRI. In 9L3.9 cells incubated with Tf-SC-CLIO, changes in T_2 relaxation times were easily detected at 90 μM iron compared to 900 μM iron for the Tf-SS-CLIO probe (Figure 6). To further demonstrate the utility of this probe, MRI was used to measure differences in ETR/TfR levels *in vivo*. Bilateral tumors with a low (9L4.2) and a high (9L3.9) expression of the TfR [7] were grown at the base of the ears of nude mice. Figure 7 shows the T_2 maps of the tumors of a representative animal superimposed with a proton-weighted MR image. MRI before contrast agent revealed no difference. However, after intravenous injection of Tf-SC-CLIO, a corresponding higher accumulation of the contrast agent in the 9L3.9 tumor led to shorter T_2 values detected by MRI. Seventy-two hours after injection of 15 mg/kg Tf-SC-CLIO, average T_2 values were 32.07 ± 5.42 milliseconds (9L3.9) and 46.94±6.43 milliseconds (9L4.2) (Table 2; Mann-Whitney *U*-test, $P < .005$). In control animals, the injection of nontargeted CLIO resulted in no differential between the two tumors at 72 hours [9L3.9 (37.17 ± 14.05 milliseconds) and 9L4.2 (38.42 ± 9.23 milliseconds), Table 2].

Imaging Differences in Endogenous TfR Expression

The next step was to investigate the feasibility and utility of MRI of endogenous levels of TfR expression after incubation with Tf-SC-CLIO. Levels of human TfR expression were measured in a panel of human breast cancer cell lines by Western blot and assessed in relation to the cell line with the highest expression, BT549 cells. All of the other malignant cell lines expressed two- to four-fold less TfR than BT549 cells (BT20, 2.9-fold less; MCF7 and HBL100, 3.4-fold less). The benign cell line, MCF10A, expressed much less TfR (118-fold less) than BT549 cells. Using these same cell lines, it was determined if these relative differences in TfR expression could be detected using Tf-SC-CLIO and MRI. The results showed a good linear correlation between the level of TfR measured by Western blot and the amount of cell-associated iron for all the cells except HBL-100 cells (correlation coefficient $r^2 = 0.94 \pm 0.07$; Figure 8). These data were confirmed by comparing the binding/uptake of [^{125}I]-Tf to the level of TfR measured by Western blot demonstrating a similarly high degree of correlation for MCF7, BT549, and MCF10A cells ($r^2 = 0.99 \pm 0.001$). Relative to BT549 cells, HBL-100 cells had less receptor but equal iron accumulation. These data point out that MR assessment of iron levels measures a complex biology encompassing multiple components including receptor levels and receptor activity, and may not be a measure of absolute receptor levels in all cases.

TfR Is an Attractive Target in Human Breast Cancers

To determine if the TfR would be an informative marker for human cancers, the extent of TfR overexpression in human breast cancer tissues was compared to nonmalignant breast tissues from the same patients. Using laser capture microdissection, matched normal and tumor tissues were isolated from 27 individual breast cancer patients, yielding 27 samples of normal breast ductal tissue, 22 invasive ductal carcinoma samples, and 17 samples of ductal carcinoma *in situ* (DCIS). RNA was isolated and amplified as described. Because the correlation between TfR mRNA and TfR receptor protein levels is well documented [24,25], we utilized RT-Q-PCR to measure the level of TfR overexpression in the patient panel. Approximately 74% of patient cancer samples overexpressed the TfR and, of these, 41% overexpressed the TfR five-fold or greater, a difference that has been demonstrated here to be measurable by MRI (Figure 9). Within this group, DCIS showed overexpression of the TfR in 35% of the samples, whereas 45% of invasive breast cancers had a five-fold or greater overexpression of TfR.

Discussion

The widespread use of early screening has the potential to reduce the risk of dying from cancer. However, the

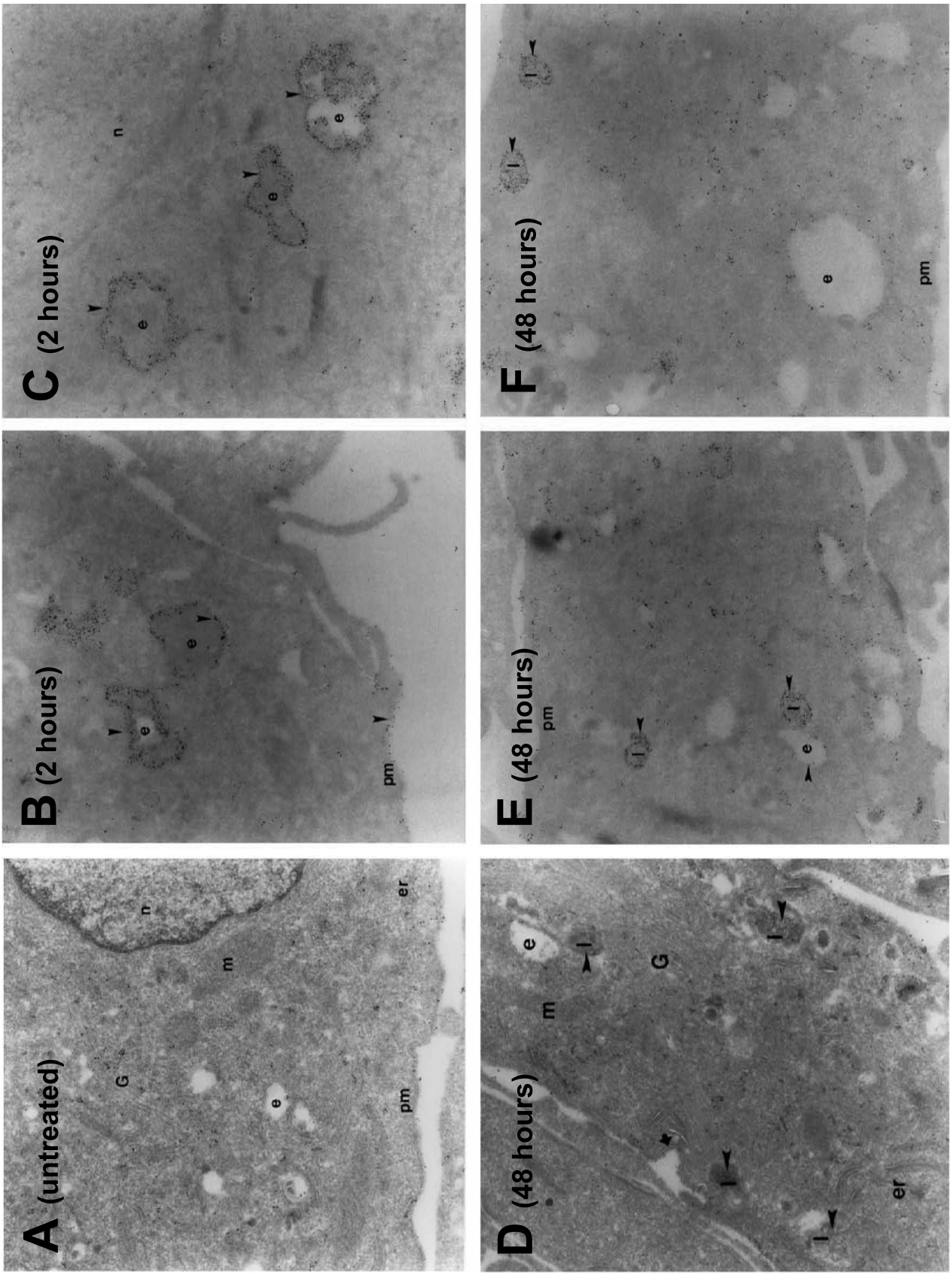
A (untreated)
n
m
er
G
e
pm
B (2 hours)
e
pm
C (2 hours)
n
e
D (48 hours)
e
m
G
er
E (48 hours)
pm
e
F (48 hours)
e
pm

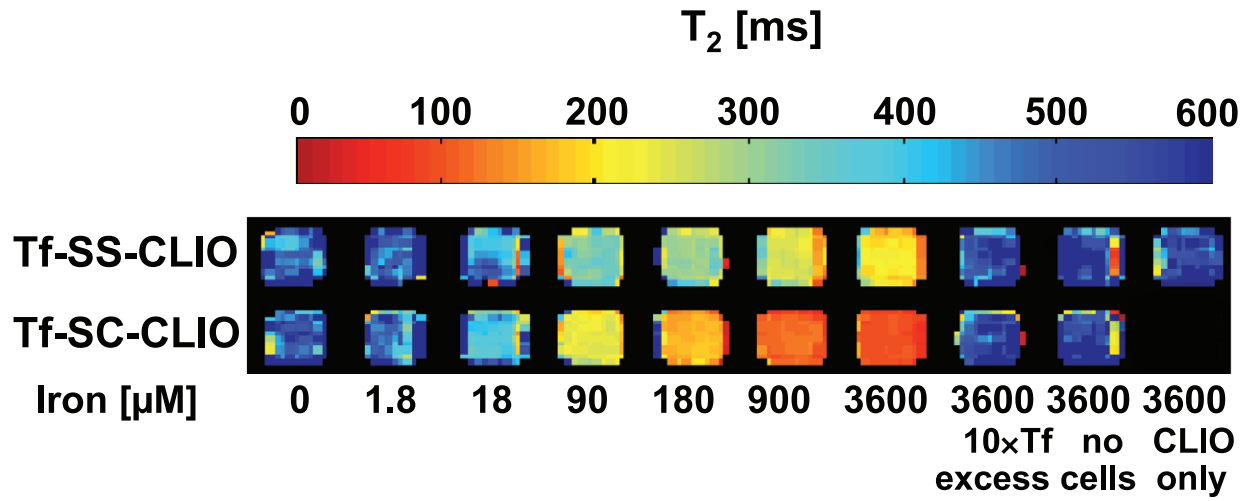

Figure 6. *MRI after incubation with different concentrations of Tf-SS-CLIO and Tf-SC-CLIO. Cells (9L3.9) were incubated with increasing concentrations of the two conjugates for 2 hours, washed, lysed, and imaged by MRI. To control for receptor specificity, cells were also incubated with nonconjugated CLIO as well as with Tf-SS-CLIO or Tf-SC-CLIO in the presence of a 10-fold excess of nonconjugated Tf. Nonspecific binding to the culture plates was measured by incubation of the probes in wells that did not contain cells. Data are shown as a color map of T_2 values.*

sensitivity of screening technologies is limited and early detection of cancer still presents an important diagnostic challenge. Detection of malignant tumor cells in a background of normal/hyperplastic benign tissues is often based on differences in physical properties between tissues, which are frequently minimal (e.g., proton relaxation times, X-ray absorption, ultrasound scattering), resulting in low contrast resolution (i.e., small tumors are not detectable). To enhance detection of small tumors, our laboratory is developing the concept of using MRI to detect the differences in molecular properties between cancer and normal tissues that arise as a result of malignant transformation.

In the studies presented here, the feasibility of using MRI to image endogenous TfR overexpression in cancer cells as a marker for human breast cancer was tested (Figure 9). The first step in these studies was to understand the interaction of the probe and target cells more completely and apply these findings to develop novel probes that would possess greater sensitivity for TfR detection. The resulting probe was used to demonstrate that the small differences in relative expression of endogenous TfR between normal and diseased tissues may be detectable using this improved probe. Laser capture microdissection and RT-Q-PCR allowed us to quantify, for the first time, the extent of TfR overexpression in a human patient population and suggests that this target may prove useful as a marker of breast cancer for MRI.

Our previous work had demonstrated that using a bifunctional linker instead of an oxidation–reduction reaction significantly increased the cellular association of Tf-targeted CLIO [8]. This increase was largely attributable to better affinity of the probe for the TfR. In the studies described here, two different linker chemistries were used to uncover that probe uptake is greater and more rapid when a thioether—rather than a disulfide—bond was used to conjugate Tf and CLIO. The greater uptake resulted in better detection by MRI and was not due to changes in affinity of the probe for TfR or altered probe efflux from the cells. Therefore, it was hypothesized that linker stability might alter the efficacy of the imaging probe by changing its cellular internalization and/or processing. When the biological stability of Tf-SS-CLIO and Tf-SC-CLIO was examined, the findings corroborated those of Feener et al. [26] in which disulfide cleavage has been demonstrated to take place at the cell surface, rather than in endosomes. The disulfide bond was labile upon 1) interaction of probe with cells even in the presence of metabolic inhibitors, or 2) after incubation with cell-conditioned medium, indicating that cleavage of Tf-SS-CLIO occurs in the culture medium and/or on the cell surface.

The improved stability of the Tf-SC-CLIO probe is probably directly responsible for the increased cellular uptake. Our data comparing the two probes suggest that cleavage of the disulfide bond releases "free" CLIO from Tf, which is poorly internalized [7–9], leading to a decrease in imaging sensitivity for the Tf-SS-CLIO probe. Furthermore, these studies are in agreement with other related studies that used TfR to introduce diagnostic or therapeutic agents into cells and found that the stability of the chemical linkage between Tf and the agent often has a major influence on the amount

Figure 5. *Analysis of uptake of iron oxide particles by electron microscopy. Results of nontreated 9L3.9 cells (panel A) and cells incubated with Tf-SC-CLIO (0.9 mM of iron) for 2 hours (panels B and C) or 48 hours (panels D, E, and F) are shown. Ultrathin sections were stained with anti–human TfR antibody conjugated to 10-nm colloidal gold, incubated with distilled water containing 2% methylcellulose and 0.4% uranyl acetate, and air-dried (panels A and D). In some experiments (panels B, C, E, and F), cell contrast was reduced by additional rinsing with distilled water and 2% methylcellulose before air drying in order to improve the discrimination of CLIO particles. Sections were examined by transmission electron microscopy and photographed at a magnification of × 21,000 (e = late endosome, l = lysosome, pm = plasma membrane, n = nucleus, G = Golgi complex, m = mitochondrion, er = endoplasmic reticulum; arrowheads indicate accumulated CLIO particles). Data demonstrate receptor-mediated accumulation of Tf-CLIO conjugates at early time points followed by a dissociation of the iron oxide particles from TfR and accumulation of the iron oxides in lysosomal compartments by 48 hours.*

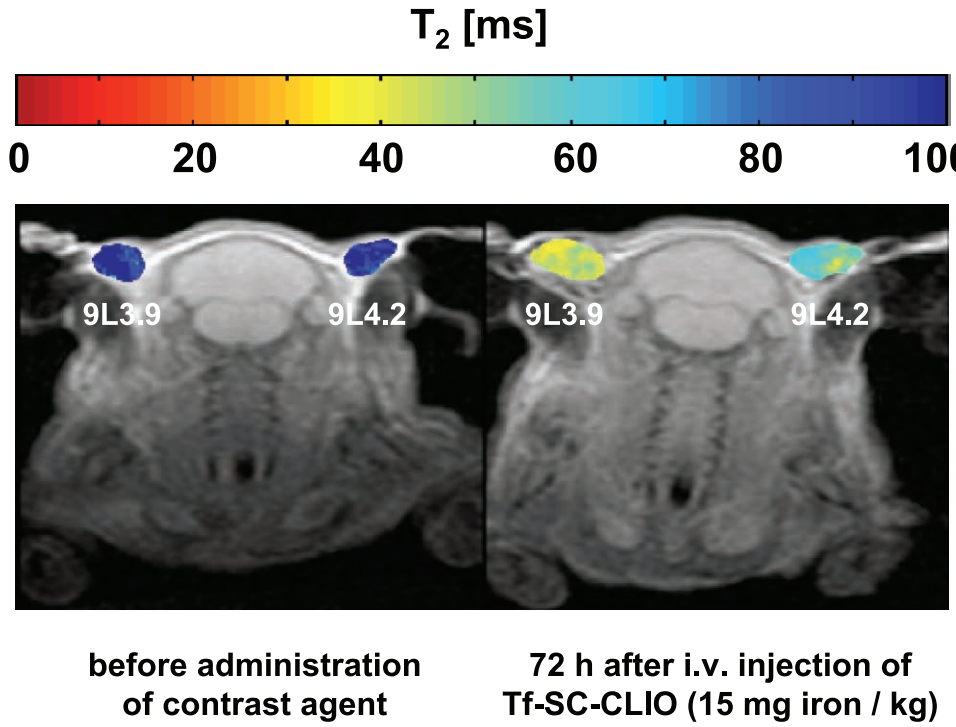

Figure 7. *Testing the Tf-SC-CLIO conjugate in vivo. Two cell lines expressing either a high (9L3.9 cells) or a low (9L4.2 cells) level of the TfR were implanted subcutaneously. Five days after implantation, MRI was performed (1.5 T, Signa 5.0, GE, 1.5-in. coil; spin echo sequence, TR 2000 milliseconds, TE 15–100 milliseconds) to generate a precontrast image. Following this precontrast MRI, Tf-SC-CLIO at a dose of 15 mg/kg iron was injected intravenously and MRI was repeated 24, 48, and 72 hours later. The T_2 values of the tumors of a representative animal superimposed with a proton-weighted image are shown. Statistical analysis of the T_2 values of four animals revealed that this difference was significant (nonparametric analysis Mann-Whitney U-test, two-tailed P value < .005).*

and/or the efficacy of the delivered conjugate [27–29]. Although these data do not rule out the possibility that the presence of more Tf ligands on the Tf-SS-CLIO (relative to Tf-SC-CLIO) probe does, in some way, impair its uptake at the cell surface, the data argue strongly that stable linker chemistry substantially influences uptake of the Tf-SC-CLIO over the Tf-SS-CLIO probe.

We were also able to follow the movement of iron oxide nanoparticles through cells over time using immunogold EM. These experiments revealed that both the Tf-SS-CLIO and Tf-SC-CLIO probes did not participate in the same intracellular pathways as the nonconjugated holotransferrin. In contrast, EM showed that the bulk of both probes was taken up by a TfR-mediated process, but was then sorted to lysosomal compartments. Compared to the 2-hour incubation, EM after 48 hours of constant incubation with imaging probes showed endosomes that were almost depleted of TfR and iron oxide particles, and lysosomes that were full of iron oxide particles. Notably, TfR was not detectable in the lysosomes, suggesting that either the receptor detaches from the probe and is sorted to a

Table 2. Time Course for T_2 Values Measured *In Vivo* for Tumors.

Tumor (hours)	CLIO		Tf-SC-CLIO	
	9L3.9	9L4.2	9L3.9	9L4.2
0	89.97 ± 45.93	84.64 ± 35.62	88.22 ± 31.74	92.66 ± 64.73
24	22.01 ± 4.56	26.76 ± 5.39	25.25 ± 8.83	23.18 ± 9.69
48	27.60 ± 3.99	31.44 ± 3.88	28.95 ± 5.34	36.74 ± 17.51
72	37.17 ± 14.06	38.42 ± 9.23	32.07 ± 5.42	46.94 ± 6.43

Average T_2 values from four animals (milliseconds) for tumors were measured as described in Experimental section. Data are reported as ± standard deviation.

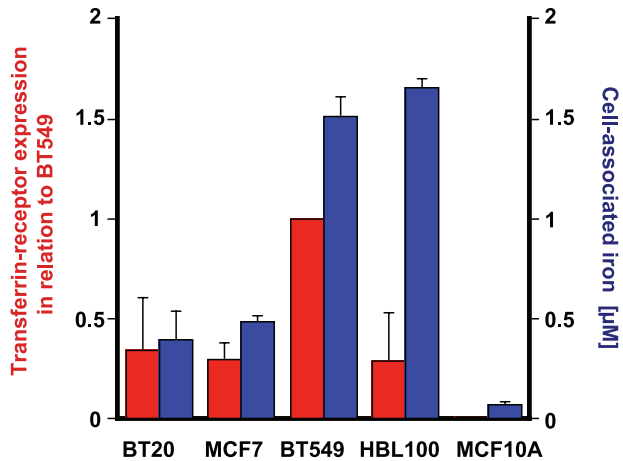

Figure 8. *Determination of TfR expression by Western blotting and cell association of Tf-SC-CLIO detected by MRI. Cells of breast cancer lines (BT20, MCF7, BT549, and HBL100) and a benign fibrocystic cell line (MCF10A) were homogenized and analyzed by Western blotting. After semiquantitative assessment using NIH image 1.6, TfR expression was calculated in relation to BT549 cells (red bars). Binding and uptake of Tf-SC-CLIO by the different cell lines was measured by MRI (blue bars) after incubation with saturating concentrations of iron (3.6 mm) and determined based on standards of purified CLIO particles.*

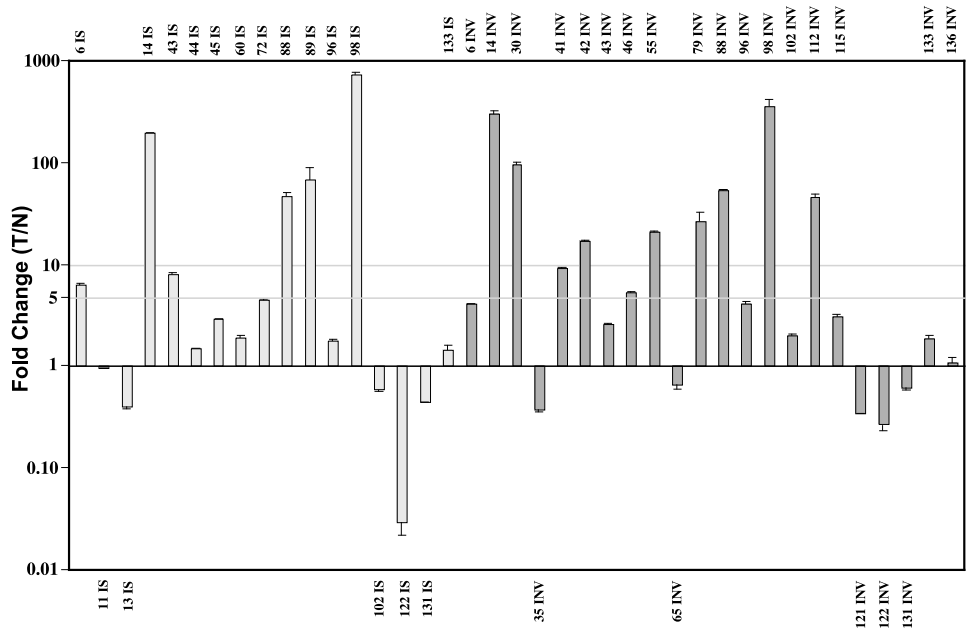

Figure 9. *Overexpression of endogenous human TfR in human breast cancer tissues and matched normal. Breast cancers from 27 different patients were microdissected and RNA was linearly amplified. Following amplification, the level of TfR mRNA was measured in RNA derived from matched normal, DCIS, or invasive cancer. Presented data report fold-change in TfR levels in either DCIS or invasive cancer, relative to matched normal breast tissue samples. Sample numbers are listed outside of the plot frame (INV = invasive ductal carcinoma, IS = ductal carcinoma in situ).*

different compartment, or that the receptor is removed by lysosomal proteases. Evidence for the latter was reported several years ago by Mellman and Plutner [30] and Mellman et al. [31]. Comparing multivalent *versus* monovalent ligands for the macrophage Fc receptor, Mellman and Plutner and Mellman et al. were able to establish that Fc receptors recycle rapidly in the presence of monovalent ligands, but were sorted to and destroyed in lysosomes when cells were treated with multivalent ligands. The multivalent nature of both imaging probes used in this study (Table 1) suggests that the probes themselves alter the processing within the cells, resulting in lysosomal retention of the nanoparticle portion of the contrast agent. These data, combined with the linker studies, strongly suggest that the major contribution to levels of Tf-SC-CLIO probe accumulated within the cells is due to linkage-dependent changes in the overall interaction and processing of the probe by the cells.

Over the years, significant literature has described the use of ^{67}Ga for imaging of cancers by the TfR, but only limited successes have been reported with most successes reported for the detection of lymphomas [32,33]. However, there are several factors that do not affect the MR probe technology presented here, but may limit ^{67}Ga imaging of the TfR. First, ^{67}Ga must bind to Tf for uptake into cells by the TfR [34–37] and, depending on the iron status of the patient, this will vary. Second, ^{67}Ga accumulates poorly within cells at a rate that is one-sixth that of ferric iron [38]. Therefore, it is likely that the recycling of the TfR causes significant efflux of internalized ^{67}Ga, limiting the radiolabel accumulation and the resulting signal that can be detected. The technology presented here does not suffer from either of these limitations as the imaging agent is conjugated to holotransferrin chemically prior to administration and the multivalency of the probe causes rerouting and vesicular accumulation of the imaging probe in cells.

To enhance the detection of small tumors, our laboratory has hypothesized that identification of imagable markers will significantly amplify the diagnostic potential of conventional imaging modalities. Our initial work demonstrated both *in vitro* and *in vivo* that MRI can be significantly improved if iron oxide nanoparticles are targeted to cell surface receptors that are overexpressed in the malignant state. However, data describing the expression patterns of such imagable markers are limited, often only reported in the literature for a few samples or qualitatively. We have now begun to identify imagable molecular markers for disease progression. Using laser capture microdissection and RT-Q-PCR, we have been able to measure the expression of these markers in matched normal and diseased tissues from patients. These studies have demonstrated that the TfR is five-fold or more overexpressed in 41% of cancers in our patient population and in even a greater percentage, 45%, of invasive breast cancers. This differential is imagable using the technologies described here. Taken together, the data presented here suggest that, although the TfR is not suitable as a stand-alone diagnostic marker, if TfR-specific probes were clinically available, they potentially would increase the sensitivity of MR for detection of small breast tumors in over 40% of cases. We are currently extending this analysis to include the larger family of internalizing receptors to determine the expression profiles of these imagable markers in cancers.

The work presented here has demonstrated that better understanding of imaging biology can significantly influence

the design, synthesis, and efficacy of MRI probes. We hope to increase our knowledge of TfR and other internalizing receptors by exploiting phage display to interrogate biology and design imaging probes that will be targeted based on peptide binding to selected sites contained within the receptors.

References

[1] Weissleder R, and Mahmood U (2001). Molecular imaging. *Radiology* **219,** 316–33.

[2] Contag CH, Jenkins D, Contag PR, and Negrin RS (2000). Use of reporter genes for optical measurements of neoplastic disease *in vivo*. *Neoplasia* **2,** 41–52.

[3] Bhaumik S, and Gambhir SS (2002). Optical imaging of *Renilla* luciferase reporter gene expression in living mice. *Proc Natl Acad Sci USA* **99,** 377–82.

[4] Gambhir SS, Herschman HR, Cherry SR, Barrio JR, Satyamurthy N, Toyokuni T, Phelps ME, Larson SM, Balatoni J, Finn R, Sadelain M, Tjuvajev J, and Blasberg R (2000). Imaging transgene expression with radionuclide imaging technologies. *Neoplasia* **2,** 118–38.

[5] Louie AY, Huber MM, Ahrens ET, Rothbacher U, Moats R, Jacobs RE, Fraser SE, and Meade TJ (2000). *In vivo* visualization of gene expression using magnetic resonance imaging. *Nat Biotechnol* **18,** 321–25.

[6] Sharma V, Luker GD, and Piwnica-Worms D (2002). Molecular imaging of gene expression and protein function *in vivo* with PET and SPECT. *J Magn Reson Imaging* **16,** 336–51.

[7] Weissleder R, Moore A, Mahmood U, Bhorade R, Benveniste H, Chiocca EA, and Basilion JP (2000). *In vivo* magnetic resonance imaging of transgene expression. *Nat Med* **6,** 351–55.

[8] Hogemann D, Josephson L, Weissleder R, and Basilion JP (2000). Improvement of MRI probes to allow efficient detection of gene expression. *Bioconjug Chem* **11,** 941–46.

[9] Moore A, Josephson L, Bhorade RM, Basilion JP, and Weissleder R (2001). Human transferrin receptor gene as a marker gene for MR imaging. *Radiology* **221,** 244–50.

[10] Moore A, Basilion JP, Chiocca EA, and Weissleder R (1998). Measuring transferrin receptor gene expression by NMR imaging. *Biochim Biophys Acta* **1402,** 239–49.

[11] Basar I, Ayhan A, Bircan K, Ergen A, and Tasar C (1991). Transferrin receptor activity as a marker in transitional cell carcinoma of the bladder. *Br J Urol* **67,** 165–68.

[12] Recht L, Torres CO, Smith TW, Raso V, and Griffin TW (1990). Transferrin receptor in normal and neoplastic brain tissue: implications for brain-tumor immunotherapy [see comments]. *J Neurosurg* **72,** 941–55.

[13] Shindelman JE, Ortmeyer AE, and Sussman HH (1981). Demonstration of the transferrin receptor in human breast cancer tissue. Potential marker for identifying dividing cells. *Int J Cancer* **27,** 329–34.

[14] Sutherland R, Delia D, Schneider C, Newman R, Kemshead J, and Greaves M (1981). Ubiquitous cell-surface glycoprotein on tumor cells is proliferation-associated receptor for transferrin. *Proc Natl Acad Sci USA* **78,** 4515–519.

[15] Trowbridge IS, and Omary MB (1981). Human cell surface glycoprotein related to cell proliferation is the receptor for transferrin. *Proc Natl Acad Sci USA* **78,** 3039–3043.

[16] Moore A, Marecos E, Bogdanov Jr A, and Weissleder R (2000). Tumoral distribution of long-circulating dextran-coated iron oxide nanoparticles in a rodent model. *Radiology* **214,** 568–74.

[17] Josephson L, Tung CH, Moore A, and Weissleder R (1999). High-efficiency intracellular magnetic labeling with novel superparamagnetic-Tat peptide conjugates. *Bioconjug Chem* **10,** 186–91.

[18] Hogemann D, Ntziachristos V, Josephson L, and Weissleder R (2002). High throughput magnetic resonance imaging for evaluating targeted nanoparticle probes. *Bioconjug Chem* **13,** 116–21.

[19] Shen T, Weissleder R, Papisov M, Bogdanov Jr A, and Brady TJ (1993). Monocrystalline iron oxide nanocompounds (MION): physicochemical properties. *Magn Reson Med* **29,** 599–604.

[20] Laemmli UK (1970). Cleavage of structural proteins during the assembly of the head of bacteriophage T4. *Nature* **227,** 680–85.

[21] Wellhoner HH, Neville Jr DM, Srinivasachar K, and Erdmann G (1991). Uptake and concentration of bioactive macromolecules by K562 cells *via* the transferrin cycle utilizing an acid-labile transferrin conjugate. *J Biol Chem* **266,** 4309–314.

[22] Peters PJ, and Hunziker W (2001). Subcellular localization of Rab17 by cryo-immunogold electron microscopy in epithelial cells grown on polycarbonate filters. *Methods Enzymol* **329,** 210–25.

[23] Sgroi DC, Teng S, Robinson G, LeVangie R, Hudson Jr JR, and Elkahloun AG (1999). *In vivo* gene expression profile analysis of human breast cancer progression. *Cancer Res* **59,** 5656–661.

[24] Casey JL, Koeller DM, Ramin VC, Klausner RD, and Harford JB (1989). Iron regulation of transferrin receptor mRNA levels requires iron-responsive elements and a rapid turnover determinant in the 3′ untranslated region of the mRNA. *EMBO J* **8,** 3693–699.

[25] Koeller DM, Horowitz JA, Casey JL, Klausner RD, and Harford JB (1991). Translation and the stability of mRNAs encoding the transferrin receptor and c-*fos*. *Proc Natl Acad Sci USA* **88,** 7778–782.

[26] Feener EP, Shen WC, and Ryser HJ (1990). Cleavage of disulfide bonds in endocytosed macromolecules. A processing not associated with lysosomes or endosomes. *J Biol Chem* **265,** 18780–785.

[27] Wagner E, Cotten M, Mechtler K, Kirlappos H, and Birnstiel ML (1991). DNA-binding transferrin conjugates as functional gene-delivery agents: synthesis by linkage of polylysine or ethidium homodimer to the transferrin carbohydrate moiety. *Bioconjug Chem* **2,** 226–31.

[28] Uike H, Sakakibara R, Iwanaga K, Ide M, and Ishiguro M (1998). Efficiency of targeted gene delivery of ligand–poly-L-lysine hybrids with different crosslinks. *Biosci Biotechnol Biochem* **62,** 1247–248.

[29] Beyer U, Roth T, Schumacher P, Maier G, Unold A, Frahm AW, Fiebig C, Unger C, and Kratz F (1998). Synthesis and *in vitro* efficacy of transferrin conjugates of the anticancer drug chlorambucil. *J Med Chem* **41,** 2701–708.

[30] Mellman I, and Plutner H (1984). Internalization and degradation of macrophage Fc receptors bound to polyvalent immune complexes. *J Cell Biol* **98,** 1170–177.

[31] Mellman I, Plutner H, and Ukkonen P (1984). Internalization and rapid recycling of macrophage Fc receptors tagged with monovalent antireceptor antibody: possible role of a prelysosomal compartment. *J Cell Biol* **98,** 1163–169.

[32] Rini JN, Manalili EY, Hoffman MA, Karayalcin G, Mehrotra B, Tomas MB, and Palestro CJ (2002). F-18 FDG *versus* Ga-67 for detecting splenic involvement in Hodgkin's disease. *Clin Nucl Med* **27,** 572–77.

[33] Bar-Shalom R, Mor M, Yefremov N, and Goldsmith SJ (2001). The value of Ga-67 scintigraphy and F-18 fluorodeoxyglucose positron emission tomography in staging and monitoring the response of lymphoma to treatment. *Semin Nucl Med* **31,** 177–90.

[34] Larson SM, Rasey JS, Allen DR, and Nelson NJ (1979). A transferrin-mediated uptake of gallium-67 by EMT-6 sarcoma: I. Studies in tissue culture. *J Nucl Med* **20,** 837–42.

[35] Motohashi H (1990). The relationship between Ga-67 uptake and transferrin receptors in cultured cells. *Kanagawa Shigaku* **24,** 618–29.

[36] Nejmeddine F, Caillat-Vigneron N, Escaig F, Moretti JL, Raphael M, and Galle P (1998). Mechanism involved in gallium-67 (Ga-67) uptake by human lymphoid cell lines. *Cell Mol Biol (Noisy-le-Grand)* **44,** 1215–220.

[37] Tsan MF (1985). Mechanism of gallium-67 accumulation in inflammatory lesions. *J Nucl Med* **26,** 88–92.

[38] Hegge FN, Mahler DJ, and Larson SM (1977). The incorporation of Ga-67 into the ferritin fraction of rabbit hepatocytes *in vivo*. *J Nucl Med* **18,** 937–39.